REVEALING SINGULARITIES IN πN and $\overline{K}$N INTERACTIONS*

R.H. LANDAU

Department of Physics, Oregon State University,
Corvallis OR 97331, USA

(Received October 9, 1996)

Data for πN and $\overline{K}$N scattering, reactions, and bound-states are examined with the chiral color dielectric model, the cloudy bag model, and a potential model. The behaviors of the T matrices in the complex energy plane as predicted by these models are used to interpret the data.

PACS numbers: 13.75. Gx, 13.75. Jz

1. Introduction

We have assembled here in Krakow to discuss the production, properties, and interactions of mesons. In this talk I will concentrate on the structure of the πN and $\overline{K}$N interactions as revealed at low energies by bound state- and resonant poles in the scattering amplitudes. This will summarize work Jeff Schnick, Guangliang He, Paul Fink, Dinghui Lu, and Shashi Phatak and I have done in which we use experimental data and a variety of calculable — but still realistic — theoretical models to provide simple views of meson-baryon interactions.

Quark models have been used extensively to study meson-baryon scattering and baryon spectra. Usually the baryon spectrum is identified with the bound-state spectrum of quarks within a potential well — even though this has two shortcomings: the influence of the meson-baryon interaction on the baryon mass is ignored and the baryons are unrealistically stable since there is no coupling to decay channels. In contrast, the experimental masses of baryons are determined as resonance energies in meson-nucleon scattering and so include shifts due to the meson-baryon interactions as well as widths due to the coupling to the open channels. For this reason it is more realistic to identify experimental masses and widths with the location

* Presented at the "Meson 96" Workshop, Cracow, Poland, May 10–14, 1996.

of the poles of the transition matrix T in the complex energy plane. [You will recall that bound states are identified with poles on the first (*physical*) energy sheet, usually on the real energy axis at energies below the threshold for scattering, and that resonances are identified with poles on the second (*unphysical*) energy sheet, the resonance being narrow if the pole is near the real axis.]

Chiral quark models, such as the cloudy bag models[1], contain mesons in additions to quarks and therefore also contain elementary meson-quark interactions. The calculation of masses with these models consequently include shifts due to the meson-baryon interactions. However, when these models use perturbation theory to calculate the widths of the excited baryons, higher-order terms are ignored and unitarity is not ensured. So again, a calculation of the poles of the transition matrix T would be preferred [2, 3].

While bag models represent a more fundamental approach to the basic physics than do the ever-popular potential models, they suffer from several limitations. First, the use of an artificial bags to confine quarks lead to coordinate-space wave functions which have sharp discontinuities at the bags' boundaries and this leads to meson-baryon form factors which have unphysical oscillations. Second, the use of static and nonrecoiling bags is unrealistic and especially so for scattering where the momentum transfers can be large. Finally, bag calculations treat the bare baryon masses and the bag radius as independent parameters even though they are related and should be fit simultaneously with the scattering data.

Chiral color dielectric models (CDM) [4] overcome some of the limitations of bag models by providing a more microscopic and dynamical mechanism for quark confinement and by including baryon recoil through nontopological-soliton solutions to the equations of motion. While the CDM was introduced only to simulate the absolute confinement of quantum chromodynamics, it was later discovered that an effective color dielectric field arises naturally in lattice QCD when coarse-grained field variables are used [5]. This color dielectric field accounts for the long-distance behavior of the QCD vacuum and produces a natural confinement of quarks within baryons [6].

Regardless of the elementary model of the two-body interaction, the calculations we undertake [3, 7, 8] contain an infinite number of higher-order terms and ensure unitarity in the meson-nucleon channels. We do that by iterating tree-level diagrams, that is, the potentials V, using the relativistic, coupled-channels, Lippmann-Schwinger equation,

$$T^{LJI}_{\beta\alpha}(k',k) = V^{LJI}_{\beta\alpha}(k',k) \; + \frac{2}{\pi} \sum_{\gamma} \int_0^{\infty} dp \, \frac{p^2 V^{LJI}_{\beta\gamma}(k',p) T^{LJI}_{\gamma\alpha}(p,k)}{E + i\epsilon - E_{\gamma}(k)} \, . \qquad (1)$$

When the input potential V consists of a bare pole times a vertex-function, the output T will have a renormalized pole together with a meson-dressed vertex function. Our work is somewhat unique in calculating the renormalized bound state spectrum and scattering simultaneously.

The subscripts α and β in (1) indicate the initial and final meson-baryon channels:

Pion Reaction			Kaon Reaction			Channel (α, β)
πN	$\rightarrow$	πN,	$K^- p$	$\rightarrow$	$K^- p$,	1
	$\rightarrow$	$\pi\Delta\,(\pi\mathrm{N}^*)$.		$\rightarrow$	$\pi\Sigma$,	2
				$\rightarrow$	$\overline{K}^o n$,	3
				$\rightarrow$	$\pi^o\Lambda^o$.	4

(2)

Since we do not include the Coulomb force for the πN system, we use an isospin basis, that is, we solve channels 1 and 2 for isospin $I = 1/2$ and $3/2$. Since we do include the Coulomb force for the $\overline{K}$N system (in order to examine kaonic hydrogen) we use a charge basis and this requires at least these four channels. Our task is to find the V to use in this equation. For the πN interaction I will show results using the chiral color dielectric quark model [7]. For the $\overline{K}$N interactions I will show results using potential models[8] and the cloudy bag model [3].

2. πN chiral color dielectric model

We use the cloudy bag model and chiral color dielectric model in similar ways to derive the $V_{\beta\alpha}^{LJI}(k', k)$ to use in (1). We start with an elementary Lagrangian containing quark and meson fields, deduce the elementary vertices (interaction Hamiltonian) by expanding the Lagrangian in powers of the meson field, and look for those pieces which produce meson-baryon interactions. Fock-space matrix elements of the appropriate Born diagrams then yield the potentials.

For our CDM calculation of the πN interaction, we start we a Lagrangian in which the quark field has already been modified so that the Weinberg–Tomozawa relation appears explicitly at the tree level [1, 4]:

$$\begin{aligned}\mathcal{L} = \; & \bar{q}\left[i\gamma^\mu D_\mu - \frac{m_q}{\chi} + \frac{1}{2f}\gamma^\mu\gamma_5\vec{\tau}\cdot D_\mu\vec{\phi} - \frac{g}{2}\lambda_a\gamma^\mu A_\mu^a\right] \\ & \times q - \frac{\kappa(\chi)}{4}(F_{\mu\nu}^a)^2 + \frac{\sigma_v^2}{2}(\partial_\mu\chi)^2 - U(\chi) + \frac{(D_\mu\vec{\phi})^2}{2} - \frac{m_\pi^2\vec{\phi}^2}{2}, \end{aligned} \tag{3}$$

where q, $\vec{\phi}$, A_μ^a and χ are the quark, meson, gluon, and dielectric fields respectively, and $\kappa(\chi) = \chi^4$ is the dielectric coefficient. The phenomenological, dielectric self-interaction field $U(\chi)$ is expressed in terms of the bag

constant B, a shape parameter α, and the dielectric field χ:

$$U(\chi) = B\alpha\chi^2\left[1 - 2\left(1 - \frac{2}{\alpha}\right)\chi + \left(1 - \frac{3}{\alpha}\right)\chi^2\right]. \tag{4}$$

Of particular interest here is the limit $\chi \to 0$ of vanishing dielectric field. Then the gluon kinetic energy term $\chi^4 F^2/4$ in the Lagrangian vanishes and the quark effective mass m_q/χ becomes infinite. Accordingly, the quark and gluon fields are confined within the baryon to the region of non-vanishing dielectric field χ. This contrasts with the bag model in which confinement is externally imposed by placing the quarks within an infinite square well.

We identify the interaction Hamiltonian by expanding the Lagrangian in powers of f^{-1}:

$$H_{int} \simeq H_{1\pi} + H_{2\pi}, \tag{5}$$

$$\begin{aligned} H_{1\pi} &= -\frac{1}{2f}\int d^3x\, \bar{q}\gamma^\mu\gamma_5\vec{\tau}q\cdot\partial_\mu\vec{\phi}, \quad H_{2\pi} \\ &= \frac{1}{4f^2}\int d^3x\, \bar{q}\gamma^\mu\vec{\tau}q\cdot\vec{\phi}\times\partial_\mu\vec{\phi}. \end{aligned} \tag{6}$$

We note that $H_{1\pi}$ has a pseudovector coupling between the pion and the quark and that $H_{2\pi}$ has a two-pion contact interaction which reproduces the Weinberg-Tomozawa result of current algebra. When we treat the baryons as composite three-quark systems and the mesons as elementary quantized fields, we obtain the hadron-space interaction Hamiltonian involving a single meson:

$$H^B_{1\pi} = \sum_{\alpha,\beta} B^\dagger_\beta B_\alpha \int \frac{d^3k\, k_\mu}{(2\pi)^{3/2}}\left[\vec{a}(k)\cdot\vec{\mathcal{V}}^\mu_{\beta\alpha}(\boldsymbol{k}) + \text{h.c.}\right], \tag{7}$$

$$H^B_{2\pi} = \sum_{\alpha,\beta} B^\dagger_\beta B_\alpha \int \frac{d^3k\, d^3k'}{(2\pi)^3}\left[\left(\vec{a}^\dagger(k')\times k_\mu\vec{a}(k)\right)\cdot\vec{\mathcal{W}}^\mu_{\beta\alpha}(\boldsymbol{k}', \boldsymbol{k}) + \text{h.c.}\right], \tag{8}$$

where $\vec{a}(k)$ is the meson annihilation operator and the vertex functions $\vec{\mathcal{V}}^\mu_{\beta\alpha}$ and $\vec{\mathcal{W}}^\mu_{\beta\alpha}$ are matrix elements of the quark pseudovector and vector current between baryon states. These Hamiltonians lead to the three distinct graphs shown in Fig. 1 which contribute in lowest order to the πN and $\pi\Delta$ potentials.

To evaluate these potentials we need know the quark fields. We get them by solving simultaneous coupled, nonlinear, partial differential equations for the quark and dielectric fields:

$$\left(i\gamma^\mu\partial_\mu - \frac{m_q}{\chi}\right)q = 0, \quad \sigma_v^2\partial_\mu\partial^\mu\chi + \frac{dU(\chi)}{d\chi} - \frac{m_q}{\chi^2}\bar{q}q = 0. \tag{9}$$

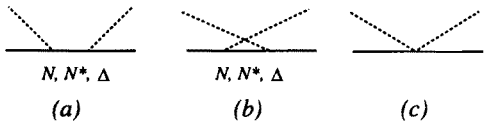

Fig. 1. The three lowest-order terms of the potential contributing to πN scattering.

We assume the dielectric field χ is time-independent and spherically symmetric, and solve numerically for χ's with soliton behaviors. The solutions of (9) describe quark orbits within baryons in which the center of mass may move. We remove this spurious motion by a Peierls-Yoccoz[9, 10] projection to form an eigenstate of momentum $\boldsymbol{p}$:

$$|B(\boldsymbol{p})\rangle = \frac{\int d\boldsymbol{r}\, e^{i\boldsymbol{p}\cdot\boldsymbol{r}}\, q^\dagger_{\boldsymbol{r}}\, q^\dagger_{\boldsymbol{r}}\, q^\dagger_{\boldsymbol{r}} e^{\int d^3k \sqrt{\frac{\omega(k)}{2}} f_{\boldsymbol{r}}(\boldsymbol{k}) a^\dagger_{gb}(\boldsymbol{k})} |0\rangle}{N_B(p)}, \tag{10}$$

where N_B is a momentum-dependent normalization constant, $q^\dagger_{\boldsymbol{r}}$ creates a quark wave function centered at $\boldsymbol{r}$, $|0\rangle$ is the vacuum state, $f_{\boldsymbol{r}}(\boldsymbol{k})$ is the Fourier transform of the scalar dielectric field $\chi(\boldsymbol{r})$, and $a^\dagger_{gb}(\boldsymbol{k})$ is the creation operator for a scalar dielectric field quanta with energy $\omega(k)$. The vertex functions with recoil corrections are evaluated between the momentum-projected baryon states in the Breit frame, for example,

$$\vec{\mathcal{V}}^\mu_{\beta\alpha}(\boldsymbol{k}) = \frac{-i\left\langle B_\beta(-\frac{\boldsymbol{k}}{2})\right| \overline{q}(0)\gamma^\mu\gamma_5\vec{\tau}q(0) \left|B_\alpha(\frac{\boldsymbol{k}}{2})\right\rangle}{2f\sqrt{2\omega_\pi(k)}}. \tag{11}$$

This vertex function is related to the axial form factor of the nucleon, with the $k \to 0$ limit of $\mathcal{V}$ determining g_A of the nucleon. We find that g_A calculated using momentum-projected states is larger than that calculated statically.

3. πN Results

We have made the important discovery that the mass and width of the Δ and nucleon are significantly affected by the closed but coupled πΔ channel. To draw this conclusion we had to simultaneously reproduce πN scattering as well as the complex energies of the nucleon and delta poles in the T matrix. As we see in Fig. 2, the numerical fitting procedure ends up with the nucleon as a single pole lying on the real energy axis (as it should since the open channels are all at higher energies), and the Δ as a

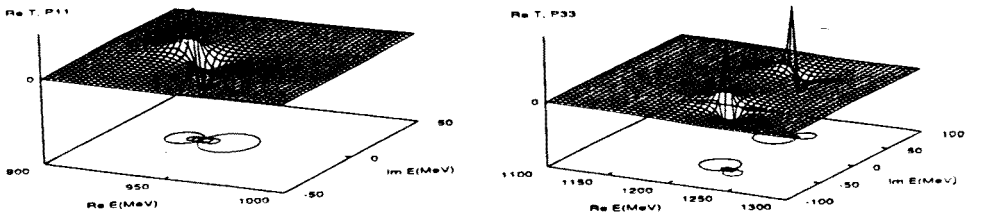

Fig. 2. The real part of the T matrix as a function of complex energy. (Left) The nucleon as a single pole on the real energy axis. (Right) The Δ as a double pole, symmetric about the real energy axis.

pair of conjugate poles (a consequence of the reflection principle for complex functions).

Somewhat surprisingly, we found that we can reproduce the experimental masses of the nucleon and delta for a bag constant $B^{1/4}$ between 100 MeV and 150 MeV and for the quark mass between 40 MeV and 120 MeV. While 40 MeV may appear small, the dielectric field also becomes small near the origin, and, consequently, the 40 MeV quark has an effective mass inside of a nucleon of $m_q/\chi(r \simeq 0) \simeq 100$ MeV. For an assumed value of the pion decay constant $f = 93\,\mathrm{MeV}$, the fitted parameters and deduced bare masses (in MeV) are $\alpha_s = 0.126$, m_{gb} =1127, $m_N^{(0)}$ =1171, and $m_\Delta^{(0)}$ =1439. The glueball mass is consistent with the values found in other models[10] and is close to the value in the particle data booklet. The effect of renormalization on the nucleon and delta masses is to move the bare masses down by $\sim 250\,\mathrm{MeV}$, a value which may get decreased if we include more repulsion in our model (a need suggested by the predicted scattering lengths).

Our study also produced renormalized and bare values for f, the pion weak decay constant, and for $f_{\pi NN}$, the πNN coupling constant. We extract the bare coupling constant $f_{\pi NN}^{(0)}$ from our final T by comparing the vertex function $v_i(k)$ computed with the CDM to the standard $g(k)$ of Chew-Low theory:

$$v_i(k) = i\sqrt{\frac{4\pi}{2\omega_k}}\frac{f_{\pi NN}^{(0)}}{m_\pi} g(k)\tau_i \boldsymbol{\sigma}\cdot k. \tag{12}$$

We extract renormalized coupling constants and renormalized form factors (Fig. 3) by making Laurent expansions of the computed T around its poles,

for example,

$$\hat{T}(k', k; E \simeq m_N) \simeq f^2_{\pi NN} \frac{g_{\pi NN}(k') g_{\pi NN}(k)}{E - m_N} + \cdots . \tag{13}$$

It is particularly interesting to compare these form factors to those of other approaches since form factors are related to the quark wave functions and are affected by the rarely-included renormalization process. We find that there is an approximate proportionality between f and $f_{\pi NN}$, and a $\sim 15\%$ renormalization effect. From the residue of T near the Δ pole we also find that

$$\frac{f_{\pi N\Delta}}{f_{\pi NN}} \simeq 1.87. \tag{14}$$

This ratio is quite close to the experimental value of ~ 2, closer in fact than the SU(6) prediction[1] of $6\sqrt{2}/5 \simeq 1.70$. This clearly shows the importance of renormalization.

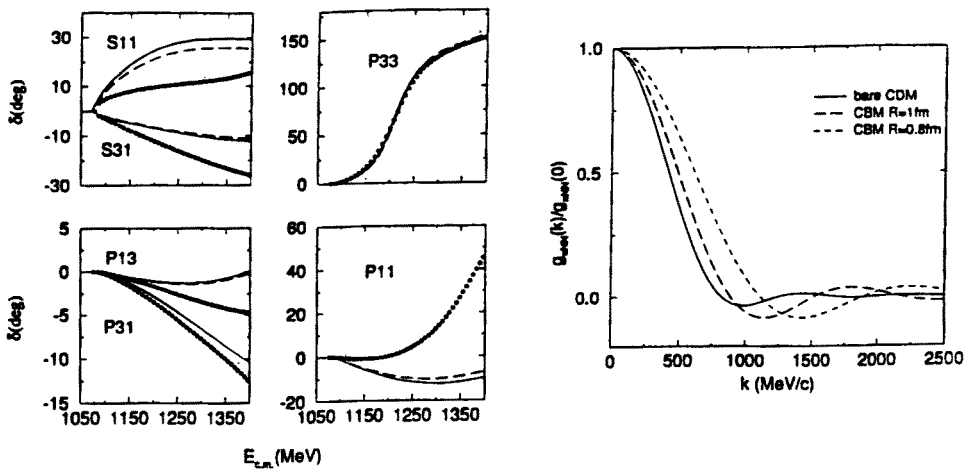

Fig. 3. (Left) The S- and P-wave πN phase shifts for f=90 and f=93. (Right) The bare πNN form factors of the color dielectric and the cloudy bag models.

On the LHS of Fig. 3 we show the πNN form factors deduced from the behavior of the T matrix near the nucleon pole. The different curves correspond to different values of the pion decay constant f. One can estimate from the falloff that the range R of the equivalent monopole form factor is approximately 0.5 fm. This R is comparable with the value $R \simeq R_{\rm bag}/\sqrt{10}$

obtained from the cloudy bag model with a bag radius $R_{\text{bag}} \simeq 1$ fm. The meson exchange models, however, use much smaller $R \sim 0.15$ fm which produces a much harder form factor. In practice, a monopole form factor falls off much slower than the form factor calculated in our model and does not fit the scattering phase shifts as well.

As shown on the RHS of Fig. 3, we find excellent agreement with the P_{33} phase shifts from threshold through the delta resonance energy, good agreement with the P_{13} and P_{31} scattering volumes, and good agreement with the energy dependence of the P_{31} phase shift for the first 300 MeV of kinetic energy. Better agreement with the S-wave and small P-wave phases requires additional repulsion in the model, possibly obtained by one-loop corrections. The model could also be improved by obtaining solutions to the field equations beyond those of the mean field approximation and by the inclusion of additional dielectric fields.

4. $\overline{K}$N Theory

The dominant characteristics of the low energy $K^- p$ interaction is the coupling of all the channels in (2) and the influence of the $\Lambda^*(1405)$ resonance in the $\Sigma\pi$ channel below the $\overline{K}$N threshold. The data for these reactions, being small in number and large in error, leave uncertainties as to whether the Λ^* is a composite $\Sigma\pi$ resonance, a $\overline{K}N$ bound state, an elementary three-quark state, or some combination of these. There is, in addition, the puzzle of the measurements of kaonic hydrogen finding the $1S$ level to have more binding than provided by the Coulomb force, which in turn implies a positive real part to the $\overline{K}N$ scattering amplitude, in contrast to the analyses of scattering data.

Schnick and Landau[8] did fit several separable potentials to the $\overline{K}N$ scattering data, and found that one could fit both the scattering and bound state data. In more recent work[3], our group has applied the cloudy bag model to the coupled channels $\overline{K}N$ interaction (2) as an improvement to potential models. The cloudy bag model work is similar to the chiral color dielectric model already described so I will avoid repetition. The cloudy bag model Lagrangian is expanded in powers of the meson field to obtain the linearized, volume–coupled, SU(3)×SU(3) Lagrangian, and this is used to deduce the potential:

$$V_{\beta\alpha} = \langle\beta|H_c|\alpha\rangle + \sum_{B_0=S01,D03,P13} \langle\beta|H_s|B_0\rangle \frac{1}{E - M_{B_0}} \langle B_0|H_s|\alpha\rangle. \qquad (15)$$

Here the first term describes direct scattering via elementary quark transitions and the second term sums over processes in which there are resonance

intermediate states. When the potential is used as the driving term in the Lippmann–Schwinger equation (1), the contact interaction potential generates composite, nonelementary resonances not present in the potential, and the elementary resonances get renormalized.

5. $\bar{K}N$ Results

We see on the LHS of Fig. 4 that Ref changes sign once below the $\bar{K}N$ threshold (right-most arrow) and for fit 1, once again slightly above the $\Sigma\pi$ threshold (left-most arrow). This is fascinating, for the ability of the model to reproduce the experimental $1S$ strong interaction shift in kaonic hydrogen depends on the magnitude and sign of Ref near threshold, and clearly there are several sign changes here. In order to unravel the mysterious resonance-like behavior of the $\bar{K}N$ scattering amplitude, we have solved for the complex energies at which the scattering amplitudes have poles. On the RHS of Fig. 4 we plot the imaginary part of the $\bar{K}N$ S wave scattering

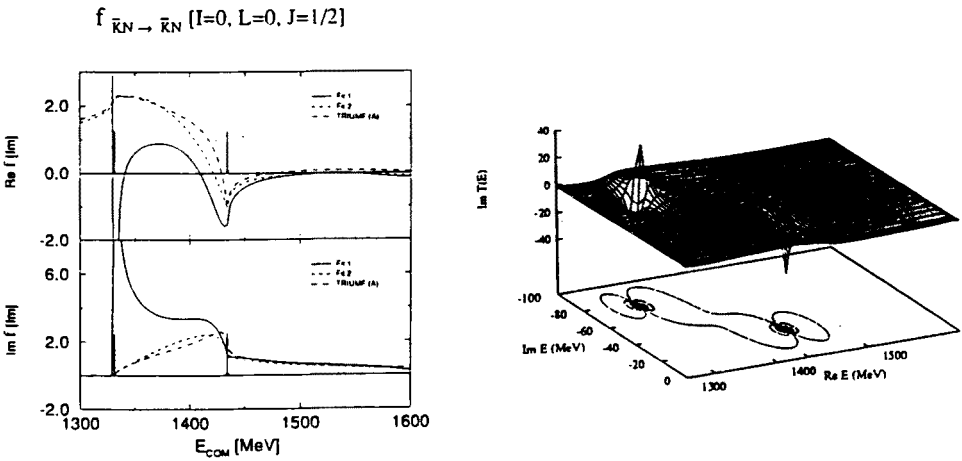

Fig. 4. (Left) The $\bar{K}N$ S_{01} scattering amplitudes for three cloudy bag model fits. The arrows show the $\Sigma\pi$ and $\bar{K}N$ thresholds. (Right) The imaginary part of the same amplitude as a function of complex energy.

amplitudes as a function of complex energy. We note two poles: a high-energy one some 17 MeV *above* the $\bar{K}N$ threshold (the tick mark to the right of 1400 MeV in the figure) and 31 MeV along the negative imaginary axis, and a low energy pole some 80 MeV below the $\bar{K}N$ threshold and far from the real energy axis (and thus of little experimental consequence). In contrast to these CBM fits, the potential models have only one S-wave pole, and it is closer to the tabulated $\Lambda(1405)$ energy. Apparently, in the

potential model, the $\Lambda(1405)$ is a composite resonance with a single pole close to its tabulated energy, while in the cloudy bag model the $\Lambda(1405)$ is not elementary and not simple.

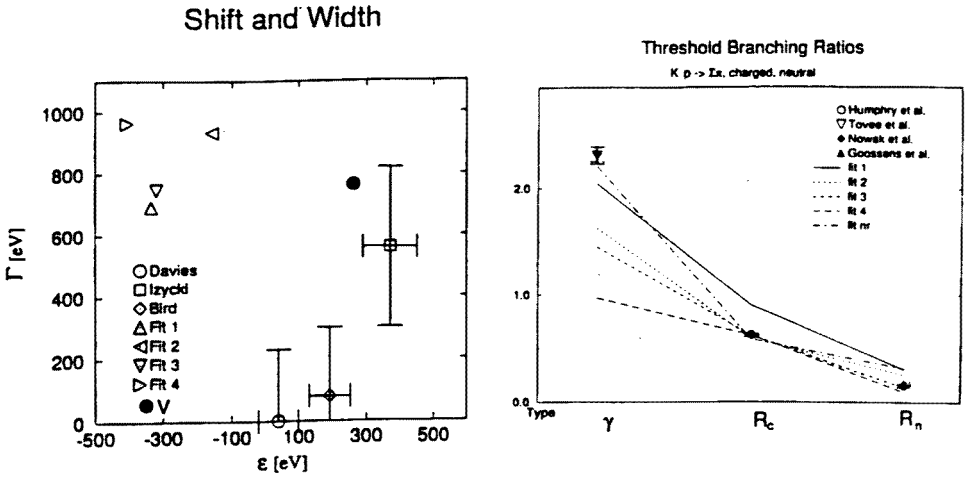

Fig. 5. (Left) The shift and width due to the strong interaction of the $1S$ level in kaonic hydrogen. The triangles are predictions of the cloudy bag model, the filled circle a prediction with the Schnick-Landau potential. (Right) The threshold branching ratios for K^-p to neutral states, to charged states, and to charged $\Sigma\pi$ states as predicted by the cloudy bag model.

The T matrices pole positions for the P and D wave amplitudes have also been calculated. In *both* cases the renormalization shifts the masses of the resonances downwards in energy by 31 MeV, considerably less than the renormalization shift in πN scattering. The tabulated masses and widths for resonances are in excellent agreement with the pole positions, while for the Σ_{P13} and Λ_{D03} there are $\sim$ 30% differences (this is expected since the widths arise completely from renormalization, and these are broad and nonsymmetric resonances).

On the LHS of Fig. 5 we show our predictions for the strong interaction shift of the 1S level in kaonic hydrogen. We calculate the binding energy by determining the complex energy poles of the T matrix for the combined Coulomb-plus-nuclear potential problem. All the CBM fits have a width which is acceptable or slightly large and a shift which is opposite in sign to the data (the experimental shifts are to the more bound). One of the potential models of Schnick and Landau[8] and its update by Tanaka and

Suzuki[11] agree in sign with the data. Although the sign changes in some of the cloudy bag model's $\mathrm{Re}f_{S01}$ are similar to those of the potential models, none have the proper combination of $I = 0$ and $I = 1$ strengths to keep $\mathrm{Re}f(K^-p) > 0$.

On the RHS of Fig. 5 we compare the cloudy bag model predictions to the experimental data for the branching ratios

$$\gamma = \frac{K^-p \to \Sigma^-\pi^+}{K^-p \to \Sigma^+\pi^-}, \quad R_c = \frac{K^-p \to \text{charged}}{K^-p \to \text{all}}, \quad R_n = \frac{K^-p \to \pi^0\Lambda}{K^-p \to \text{neutral}}. \tag{16}$$

We see that some of the cloudy bag model fits can reproduce these ratios adequately, although they generally are not the ones which reproduce the the $K^-p \to (\Sigma\pi\pi\pi, \Lambda\pi\pi\pi)$ mass spectra well. Although not shown, the potential model of Tanaka and Suzuki[11] agree well with these ratios.

6. Conclusions

We have witnessed a progression in the sophistication of theory used to understand meson-baryon interactions: from potential models, to bag models, to color dielectric models. We now have included natural and realistic quark confinement, baryon recoil, and the dominant coupled two-body channels. We use model field theories to derive effective potentials containing terms up to second order in the meson-baryon coupling, and then use these potentials as input to relativistic, coupled-channels Lippmann-Schwinger equations. In this way we derive renormalized values for coupling constants, form factors, and resonance masses. We find much success for such simple models. They can be improved by including higher order terms which will give added repulsion, by solving the field equations with more accuracy than afforded by the mean field approximation, and by the inclusion of additional dielectric fields.

This work is supported in part by the United States Department of Energy under grants DE-FG03-96ER40966 and DE-FG06-86ER40283.

REFERENCES

[1] A.W. Thomas, *Adv. Nucl. Phys.* **13**, 1 (1984); G.A. Miller, *Int. Rev. Nucl. Phys.*, edited by W. Weise, **1** (1984).

[2] A.W. Thomas, S. Theberge, G.A. Miller, *Phys. Rev.* **D24**, 216 (1981); E.A. Veit, B.K. Jennings, A.W. Thomas, *Phys. Rev.* **D33**, 1859 (1986).

[3] G. He, R.H. Landau, *Phys. Rev.* **C48**, 3047 (1993).

[4] S. Sahu, S.C. Phatak, *Mod. Phys. Lett.* **A7**, 709 (1992); S. Sahu, Ph. D. Thesis, Uktal University, Bhubaneswar.

[5] H.B. Nielsen, A. Patkos, *Nucl. Phys.* **B195**, 137 (1982).

[6] G. Krein, P. Tang, L. Wilets, A.G. Williams, *Nucl. Phys.* **A523**, 548 (1991).

[7] D. Lu, S.C. Phatak, R.H. Landau, *Phys. Rev.* **C51**, 2207 (1995).

[8] J. Schnick, R.H. Landau, *Phys. Rev. Lett.* **58**, 1719 (1987); P.J. Fink, G. He, R.H. Landau, J.W. Schnick, *Phys. Rev.* **C41**, 2720 (1990).

[9] R.E. Peierls, J. Yoccoz, *Proc. Phys. Soc.* (London), **A70**, 381 (1957).

[10] L. Wilets, *Non-Topological Solitons*, World, Singapore 1989; M.C. Birse, *Prog. Part. Nucl. Phys.* **25**, 1 (1990).

[11] K. Tanaka, A. Suzuki, *Phys. Rev.* **C45**, 2068 (1992).